

Supplemental Materials for
Deepening roots can enhance carbonate weathering
Submitted to Biogeosciences

5 Hang Wen¹, Pamela L. Sullivan², Gwendolyn L. Macpherson³, Sharon A. Billings⁴, Li Li^{1*}

¹Department of Civil and Environmental Engineering, Pennsylvania State University, University Park PA 16802, United States

10 ²College of Earth, Ocean, and Atmospheric Science, Oregon State University, Corvallis OR 97331, United States

³ Department of Geology, University of Kansas, Lawrence KS 66045, United States

⁴ Department of Ecology and Evolutionary Biology and Kansas Biological Survey, University of Kansas, Lawrence KS 66045, United States

15 * *Correspondence to:* Li Li (lili@engr.psu.edu)

Address: Dept. of Civil and Environmental Engineering, The Pennsylvania State University, University Park, PA 16802, United States

Phone: (814) 867-0151

20

The supplemental materials contain the detailed description of the study site Konza, and field and laboratory methods, the setup of reactive transport modeling, calculation of reactive transport times for Figure 6, derivation of equations for Ca and DIC concentrations, and carbonate chemistry data from fields for Figure 7.

25

S1. Description of the study site

Konza is a mesic native grassland where long-term (42 yrs, 2019) burning regime experiments across 60 watersheds has resulted in the encroachment of woody vegetation mostly in the riparian zone (Veach et al., 2014; Vero et al., 2018) (Figure S1). The average annual air temperature and precipitation is 13°C and ~835 mm, respectively (Nippert and Knapp, 2007; Hayden, 1998). The growing season is from April to September, when 75% of the annual precipitation occurs. Konza also has frequent storms in almost any time of a year (Hayden, 1998). The bedrock of Konza contains repeating Permian couplets of 1-2 m thick limestone and slightly thicker mudstone (2-4 m) units (Macpherson, 1996). Limestone units are composed of primarily calcite with traces of dolomite (Macpherson et al., 2008), whereas mudstones are dominated by illite, chlorite, and mixed-layer clays of chlorite-illite and chlorite-vermiculite, varying in abundance from major to trace amounts (Macpherson and Sullivan, 2019). With an average thickness of 1-2 m in the lowlands, soils mostly have carbonate minerals less than 25% with moderately low cation exchange capacities (Ransom et al., 1998). The soil is relatively thick and the water table is shallow so the response of groundwater to recharge events is rapid (Tsypin and Macpherson, 2012).

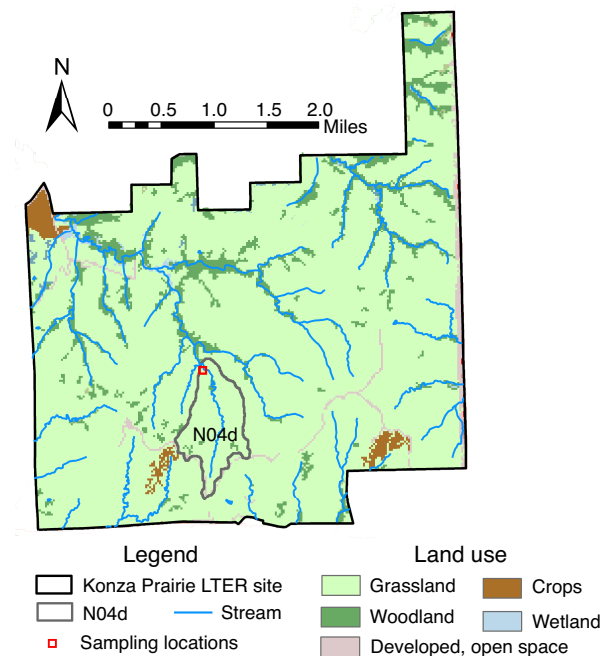


Figure S1. (A) Map of the Konza Prairie Long-Term Ecological Research (LTER) site. We used data from N04d to parameterize the model.

Most of the Konza Prairie consists of grass species (e.g., big bluestem, *Andropogon gerardii*; little bluestem, *A. scoparius*; Indiangrass, *Sorghastrum nutans*; and switchgrass, *Panicum virgatura*) and native
50 riparian gallery forest (oak, *Quercus spp.*; hackberry, *Celtis occidentalis*; and elm, *Ulmus Americana*)
(Freeman, 1998). Watersheds with fire frequency return intervals of ~4 years or greater have incurred
significant increase in woody vegetation on the hillslopes (e.g., dogwood, *Cornus drummondii*; sumac,
Rhus glabra) and a pronounced increase in woody riparian vegetation (Veatch et al., 2014) since the
inception of the experimental design (Briggs et al., 2005).

55

S2. Field and laboratory methods

All field observation wells were made of 5-cm-diameter PVC pipe. Sampling occurred monthly
during 2009-2010. Soil water was collected through soil-water samplers (Model 1900, Soil Moisture
60 Equipment Co.) at three horizons, including 17, 153, and 366 cm. Soil gas wells were established at depths
of 16, 84 and 152 cm so that the bottom hole of the gas well was at the same level as the midpoint of the
water sampler's cup. 200 mL of soil gas was collected through a vacuum pump with Tygon® tubing into a
12 mL Exetainer® glass vial. More details are referred to Tsypin and Macpherson (2012).

Alkalinity of water samples was determined by titration with 0.02 N H₂SO₄. Concentrations of Cl
65 were determined by suppressed ion chromatography (IC) with a Dionex 4000i (AG4A-SC and AS4A-SC
columns and anion self-regenerating suppressor). Cations (Ca²⁺, Mg²⁺, Na⁺ and K⁺) and dissolved Si
(H₄SiO₄(aq)) were measured by inductively-coupled plasma-optical emission spectroscopy (JY 138 Ultrac
ICP-OES) (detailed in Tsypin and Macpherson (2012)). Concentration of CO₂(g) in the samples of soil gas
was measured with an Agilent Technologies 6890N Gas Chromatograph.

70

S3. Model setup

Base case scenario with Konza field data. Soil mineralogy data indicated that as soil depth increases, anorthite ($CaAl_2Si_2O_8(s)$) and K-feldspar ($KAlSi_3O_8(s)$) decrease from 5.0% (v/v soil phase) to 0 while calcite ($CaCO_3(s)$) increases from 0 to 10.0% (v/v) (Wehmueller et al., 1993;Gunal and Ransom, 2005). Quartz and illite were relatively constant at around 40.0% (v/v) (Table S1). For the base case model, the shallow soils included anorthite, K-feldspar, and kaolinite in addition to calcite. Based on the average temperature measured at the top (soil surface) and bottom (groundwater) during the sampling period (Tsy-pin and Macpherson, 2012), soil temperature was assumed to decrease linearly with depth from 17 °C to 8 °C.

Table S1. Initial soil water chemistry, mineral compositions in different layers ^a

Chemical species	Initial soil water chemistry					Ways obtained
Aqueous species (mol/L except pH)	Rainwater	Horizon A (h = 17 cm)	Horizon AB (84 cm)	Horizon B (152 cm)	Groundwater (366 cm)	
pH ^b	6	6	6.2	6.8	7.0	Estimated ^b
Alkalinity	2.09×10^{-3}	2.09×10^{-3}	-	2.09×10^{-3}	2.09×10^{-3}	Measured
CO ₂ (aq)	1.23×10^{-5}	1.14×10^{-3}	1.74×10^{-3}	2.06×10^{-3}	8.54×10^{-4}	Estimated ^c
Cl	5.00×10^{-6}	1.74×10^{-3}	-	1.55×10^{-3}	6.06×10^{-4}	Measured
H ₄ SiO ₄ (aq)	1.00×10^{-4}	8.39×10^{-4}	-	7.89×10^{-4}	2.80×10^{-4}	Measured
Ca	2.06×10^{-5}	3.18×10^{-3}	-	3.75×10^{-3}	2.35×10^{-3}	Measured
Mg	1.00×10^{-6}	7.50×10^{-4}	-	9.04×10^{-4}	8.54×10^{-4}	Measured
Na	2.15×10^{-5}	3.39×10^{-3}	-	2.31×10^{-2}	4.35×10^{-4}	Measured
K	1.53×10^{-6}	3.97×10^{-4}	-	2.54×10^{-4}	2.09×10^{-4}	Measured
Gas						
CO ₂ (g) (%)		3.60	6.10	6.70	2.70	Measured
Mineral Volume Fraction (m ³ /m ³)	h=0-54 cm	55-98 cm	99-145 cm	146-180 cm	181-366 cm	
Quartz	4.0×10^{-1}	4.0×10^{-1}	4.0×10^{-1}	4.0×10^{-1}	4.0×10^{-1}	Measured
Anorthite	5.0×10^{-2}	5.0×10^{-2}	5.0×10^{-2}	4.0×10^{-2}	0	Measured
Orthoclase	5.0×10^{-2}	5.0×10^{-2}	5.0×10^{-2}	4.0×10^{-2}	0	Measured
Calcite	0	5.0×10^{-3}	1.0×10^{-2}	1.5×10^{-2}	1.0×10^{-1}	Measured
Illite	4.0×10^{-1}	4.0×10^{-1}	4.0×10^{-1}	4.0×10^{-1}	4.0×10^{-1}	Measured
Kaolinite	1.0×10^{-1}	1.0×10^{-1}	1.0×10^{-1}	1.0×10^{-1}	1.0×10^{-1}	Measured

a. Initial species concentrations in soil water and CO₂(g) at measured horizon layers were from (Tsy-pin and Macpherson, 2012); The corresponding concentrations between measured horizon layers were interpolated linearly; Mineralogy composition were referred to (Macpherson, 1996;Macpherson et al., 2008).

b. The pH values in soil water were determined using measured alkalinity $C_A = C_{HCO_3^-} + 2C_{CO_3^{2-}} + C_{OH^-} - C_{H^+}$,

$$C_{HCO_3^-} = \frac{C_{CO_2(aq)}K_2}{C_{H^+}} \text{ and } C_{CO_3^{2-}} = \frac{C_{HCO_3^-}K_3}{C_{H^+}}.$$

c. CO₂(aq) concentrations were estimated through Henry's law $C_{CO_2(aq)} = K_1pCO_2$.

Rainfall chemistry is relatively constant across the year (Table S1). The initial conditions were estimated through a linear interpolation with depth based on the measurements at the three sampling locations (Figure 2A), including Horizon A (depth from the soil surface $h = 17$ cm), Horizon AB ($h = 84$ cm), Horizon B ($h = 152$ cm), and Groundwater ($h = 366$ cm). The initial $\text{CO}_2(\text{aq})$ concentrations at the sampling locations were estimated using Henry's law, i.e., $C_{\text{CO}_2, \text{reference}(\text{aq})} = K_1 p \text{CO}_2 \text{reference}$. The K_1 was temperature-dependent, following the van't Hoff equation:

$$K(T) = K_{25} \exp \left(-\frac{\Delta H^\circ}{R} * \left(\frac{1}{T} - \frac{1}{273.15 + 25} \right) \right) \quad (\text{S1})$$

Here K_{25} is the solubility in water at 293.15 K (25 °C); ΔH° is the standard enthalpy of the reaction and R is the gas constant ($= 8.314 \times 10^{-3}$ kJ/K/mol); T is Kelvin temperature (K). For the dissolution of $\text{CO}_2(\text{g})$ (Reaction 1 in Table 1), $K_{1,25}$ (i.e., Henry's law constant) and ΔH_1° is 3.4×10^{-2} mol/kg/atm and -19.98 kJ/mol, respectively (Linstrom and Mallard, 2001).

In the model, $C_{\text{CO}_2(\text{aq})}$ values were used as the “equilibrium constant” in the CrunchTope database for the combined reactions 0-1 (in Table 1) to become $\text{CO}_2(\text{g}^*) \leftrightarrow \text{CO}_2(\text{aq})$. And as the parameter used to control the soil $p\text{CO}_2$ level in the model, the prescribed $C_{\text{CO}_2(\text{aq})}$ value was both temporally- and spatially-dependent in the base case. The $C_{\text{CO}_2(\text{aq})}$ values at different depths were interpolated linearly based on the estimation ($C_{\text{CO}_2(\text{aq})} = K_1 p\text{CO}_2$) at three sampling layers with monthly soil CO_2 data (Table 2). With an assumed linearly decreasing relationship with soil depth, soil temperature along depth was used as a track for CrunchTope and its database to obtain the $C_{\text{CO}_2(\text{aq})}$ value for the corresponding soil depth. The $C_{\text{CO}_2(\text{aq})}$ values along depth (associated linearly with soil temperature) were updated monthly through multiple CrunchTope database files (each month with one updated $C_{\text{CO}_2(\text{aq})}$ database) through the CrunchTope “restart” and “save_restart” option. Thus, through the prescribed temporally (monthly) and spatially (depth) dependent $C_{\text{CO}_2(\text{aq})}$, the soil $p\text{CO}_2$ concentrations were well simulated in the model compared to field data and further determined the dynamics of Ca and DIC, as have been shown in Section 4.1 and 5.1.

S4. Calculation of reactive transport times for Figure 6

In the term $kA_T \left[1 - \exp\left(-\frac{\tau_{eq}}{\tau_a}\right)\right]$, $k_{calcite}$ is the intrinsic calcite kinetic rate constant measured under well-mixed conditions ($10^{-7.69}$ mol/m²/s, Table 1) while A_T is total calcite surface area (m³); τ_{eq} is the time for a mineral to reach equilibrium in a closed, well-mixed system: $\tau_{eq} = \frac{V_T \phi (C_{eq} - C_0)}{A_T k}$, where V_T is the total domain volume (m³); C_{eq} and C_0 are the equilibrium and initial Ca concentration (mol/m³) respectively. For the cases with annual-average soil CO₂ in Scenario 1-3, C_{eq} was ~1.6 mol/m³ (as shown in Figure 3) and τ_{eq} was estimated to be $10^{-4.34}$ yr (0.40 hours). For the Konza base case, monthly soil CO₂ in September and March had the highest and lowest values respectively (Table 2), leading to corresponding equilibrium Ca concentrations and therefore different τ_{eq} values. The τ_{eq} in September and March was estimated to be $10^{-4.29}$ and $10^{-4.42}$ yr, respectively. In the heterogeneity factor $\left\{1 - \exp\left[-L\left(\frac{\tau_a}{\tau_{ad,r}}\right)\right]\right\}^\alpha$, the shape factor α is determined by physical heterogeneity given by the permeability contrast between reactive and non-reactive zones. For the different flow partitioning cases, grassland (95% vs. 5%) vs. woodland (60% vs. 40%), we assumed $\alpha = 0.8$ to represent a high heterogeneous field. The $\frac{\tau_a}{\tau_{ad,r}}$ quantifies the relative timescale of advection in the whole domain (residence time $\tau_a = \frac{L\phi}{Q_T}$) versus transport time in reactive zones ($\tau_{ad,r}$). The $\tau_{ad,r} = \frac{\tau_{a,r}\tau_{d,r}}{\tau_{a,r} + \tau_{d,r}}$ quantifies the transport time coupling diffusion/dispersion and advection in the calcite zones, where $\tau_{a,r}$ and $\tau_{d,r}$ are the average timescale of advection and diffusion/dispersion in the calcite zone, respectively. When $\frac{\tau_a}{\tau_{ad,r}} > 1$, reaction products transport out of the calcite zones faster than the domain residence time, leading to the negligible mass transport limitation caused by preferential flow paths and values of heterogeneity factor $\left\{1 - \exp\left[-L\left(\frac{\tau_a}{\tau_{ad,r}}\right)\right]\right\}^\alpha$ approaching 1.0. In contrast, when $\frac{\tau_a}{\tau_{ad,r}} < 1$, water mostly bypasses the reactive calcite zones, leading to significant influence of flow partitioning and the heterogeneity factor $\ll 1.0$. Calculated τ_a , $\tau_{a,r}$, $\tau_{d,r}$, and $\tau_{ad,r}$ and their corresponding weathering rates

for Scenarios 1-3 are in Table S2. The calcite weathering rates (mol/yr) are equivalent to the effluent Ca
 135 fluxes (shown in Figure 4).

Table S2. Calculated timescales in the grassland and woodland cases under different infiltration rates

Cases	Infiltration rate (m/yr)	τ_a (year)	$\tau_{a,r}$ (year)	$\tau_{d,r}$ (year)	$\tau_{ad,r}$ (year)	$\frac{\tau_a}{\tau_{ad,r}}$	$R_{calcite}$ (mol/yr)
Grass _{PF}	$10^{-1.4}$	4.7×10^1	8.0×10^2	4.7×10^2	2.9×10^2	1.6×10^{-1}	3.9×10^{-2}
Wood _{PF}			1.0×10^2	4.7×10^2	8.2×10^1	5.6×10^{-1}	4.6×10^{-2}
Grass _{VF}			4.0×10^1	4.7×10^2	4.0×10^1	1.3×10^0	5.9×10^{-2}
Wood _{VF}			4.0×10^1	4.7×10^2	4.0×10^1	1.3×10^0	6.0×10^{-2}
Grass _{HF}			0	4.7×10^2	4.7×10^2	1.0×10^{-1}	3.4×10^{-2}
Wood _{HF}			0	4.7×10^2	4.7×10^2	1.0×10^{-1}	3.3×10^{-2}
Grass _{PF}	$10^{-0.4}$	4.7×10^0	8.0×10^1	4.7×10^2	6.8×10^1	6.9×10^{-2}	1.8×10^{-1}
Wood _{PF}			1.0×10^1	4.6×10^2	9.8×10^0	4.8×10^{-1}	3.4×10^{-1}
Grass _{VF}			4.0×10^0	4.6×10^2	4.0×10^0	1.2×10^0	5.7×10^{-1}
Wood _{VF}			4.0×10^0	4.6×10^2	4.0×10^0	1.2×10^0	5.9×10^{-1}
Grass _{HF}			0	4.7×10^2	4.7×10^2	1.0×10^{-2}	1.2×10^{-1}
Wood _{HF}			0	4.7×10^2	4.7×10^2	1.0×10^{-2}	1.4×10^{-1}
Grass _{PF}	$10^{0.6}$	4.7×10^{-1}	8.0×10^0	4.6×10^2	7.8×10^0	6.9×10^{-2}	7.9×10^{-1}
Wood _{PF}			1.0×10^{-1}	4.4×10^2	1.0×10^0	4.7×10^{-1}	2.4×10^0
Grass _{VF}			4.0×10^{-1}	4.0×10^2	4.0×10^{-1}	1.2×10^0	5.3×10^0
Wood _{VF}			4.0×10^{-1}	4.0×10^2	4.0×10^{-1}	1.2×10^0	5.6×10^0
Grass _{HF}			0	4.7×10^2	4.7×10^2	1.0×10^{-3}	3.9×10^{-1}
Wood _{HF}			0	4.7×10^2	4.7×10^2	1.0×10^{-3}	3.4×10^{-1}

S5. Derivation of equations for thermodynamics of calcite dissolution and the dependence of 140 equilibrium C_{Ca} and C_{DIC} on soil CO_2 and temperature

Combining Reactions 1 and 4 in Table 1, the overall reaction is $CaCO_3(s) + CO_{2(g)} + H_2O \leftrightarrow$

$Ca^{2+} + 2HCO_3^-$, with its equilibrium constant can be expressed as:

$$K_t = \frac{a_{Ca^{2+}} a_{HCO_3^-}^2}{pCO_2} = K_1 K_4 \quad (S2)$$

The solutes follow the charge balance:

$$2C_{Ca^{2+}} + C_{H^+} = C_{HCO_3^-} + C_{OH^-} + 2C_{CO_3^{2-}} \quad (S3)$$

With the soil water pH typically lower than 8.3, $C_{CO_3^{2-}}$, C_{OH^-} , and C_{H^+} are negligible, such that the above
 equation can be simplified into

$$2C_{Ca^{2+}} = C_{HCO_3^-} \quad (S4)$$

Assuming relatively low salinity, activities are close to concentrations, the combination of Eq. S2 and S4

yield:

$$C_{Ca^{2+}} = \sqrt[3]{\frac{K_t \cdot pCO_2}{4}} \quad (S5)$$

$$C_{DIC} = C_{CO_2(aq)} + C_{HCO_3^-} + C_{CO_3^{2-}} \approx 2\sqrt[3]{\frac{K_t \cdot pCO_2}{4}} + K_1 \cdot pCO_2 \quad (S6)$$

Equilibrium constants are temperature-dependent and can be estimated using the van't Hoff equation (Eq. S1), the total equilibrium constant $K_t (= K_1 K_4)$ can be estimated as:

$$K_t(T) = K_{t,25} \exp\left(-\frac{\Delta H_t^\circ}{R} * \left(\frac{1}{T} - \frac{1}{273.15+25}\right)\right) \quad (S7)$$

Here $K_{t,25} (=K_{1,25} K_{4,25})$, listed in Table 1) is $10^{-6.59}$ and $10^{-5.99}$ for “impure” and “pure” calcite, respectively;

Note that the $K_{t,25}$ for “impure” calcite may vary by locations with differently mineralogy (Macpherson and Sullivan, 2019) and for this work was calibrated based on the data-model fit (Ca and alkalinity concentrations). The standard enthalpy $\Delta H_t^\circ (= \Delta H_1^\circ + \Delta H_4^\circ)$, listed in Table 1) is -35.83 kJ/mol. This

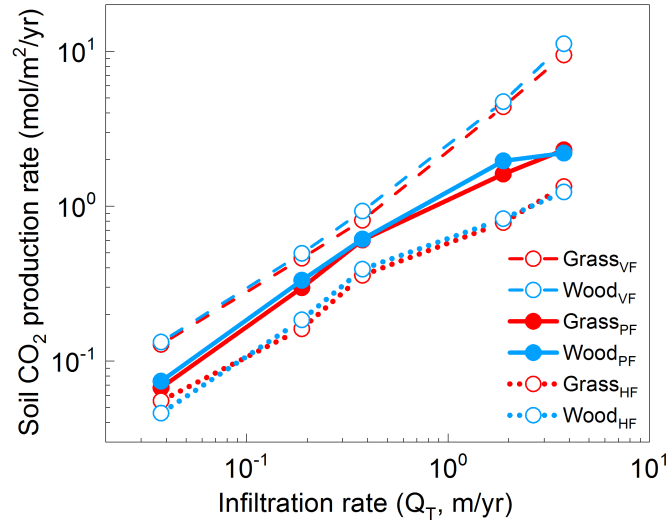
suggests that the concentrations of Ca and DIC can be estimated directly through temperature and pCO_2 as follows:

$$C_{Ca} = \sqrt[3]{K_{t,25} \exp\left(-\frac{\Delta H_t^\circ}{4R} * \left(\frac{1}{T} - \frac{1}{273.15+25}\right)\right) \cdot pCO_2} \quad (S8)$$

$$C_{DIC} = 2\sqrt[3]{K_{t,25} \exp\left(-\frac{\Delta H_t^\circ}{4R} * \left(\frac{1}{T} - \frac{1}{273.15+25}\right)\right) \cdot pCO_2} + K_{1,25} \exp\left(-\frac{\Delta H_1^\circ}{4R} * \left(\frac{1}{T} - \frac{1}{273.15+25}\right)\right) \cdot pCO_2 \quad (S9)$$

165 Here $K_{t,25}$ is equilibrium constant $K_t = \frac{a_{Ca^{2+}}a_{HCO_3^-}^2}{pCO_2} = K_1K_4$ at 25°C; ΔH° is the standard enthalpy; R is the gas constant ($=8.314 \times 10^{-3}$ kJ/K/mol); T is Kelvin temperature (K). Eq. S8 and S9 suggest that Ca and DIC concentrations can be estimated directly from temperature, pCO_2 , and thermodynamics (ΔH_t°).

170 **S6. Carbonate chemistry data for Figure 7.** These catchments meet the criteria of carbonate water chemistry: $(Ca + Mg)/alkalinity$ molar ratio < 0.9 , $Ca/SO_4 > 10$, $Ca/Na > 12$, $Ca/Mg > 1$, and charge balance error $< 10\%$ (Romero-Mujalli et al., 2019; Gaillardet et al., 1999). Overall, there are 162 data points, including pCO_2 , Ca and DIC concentrations in spring water. The concentrations of $CO_2(g)$, Ca and DIC in spring water were assumed to be similar to those in groundwater, which are often difficult and expensive
175 to obtain.



180 Figure S2. Soil CO_2 production rate as a function of infiltration rate under steady state in numerical experiments: $Grass_{PF}$ and $Wood_{PF}$ with flow partitioning, $Grass_{VF}$ and $Wood_{VF}$ with 100% vertical flow (no flow partitioning), and $Grass_{HF}$ and $Wood_{HF}$ with 100% lateral flow (no flow partitioning).

Reference

- Briggs, J. M., Knapp, A. K., Blair, J. M., Heisler, J. L., Hoch, G. A., Lett, M. S., and McCarron, J. K.: An ecosystem in transition. Causes and consequences of the conversion of mesic grassland to shrubland, *Bioscience*, 55, 243-254, 10.1641/0006-3568(2005)055[0243:Aeitca]2.0.Co;2, 2005.
- Freeman, C. C.: The flora of Konza Prairie: a historical review and contemporary patterns, *Grassland dynamics: long-term ecological research in tallgrass prairie*. Oxford University Press, New York, 69-80, 1998.
- Gaillardet, J., Dupré, B., Louvat, P., and Allègre, C. J.: Global silicate weathering and CO₂ consumption rates deduced from the chemistry of large rivers, *Chem. Geol.*, 159, 3-30, 10.1016/S0009-2541(99)00031-5, 1999.
- Gunal, H., and Ransom, M. D.: Clay mineralogy, specific surface area and micromorphology of polygenetic soils from Eastern Kansas, *Archives of Agronomy and Soil Science*, 51, 459-468, 2005.
- Hayden, B. P.: Regional climate and the distribution of tallgrass prairie, *Grassland dynamics: long-term ecological research in tallgrass prairie*. Oxford University Press, New York, 19-34, 1998.
- Linstrom, P. J., and Mallard, W. G.: NIST Chemistry webbook; NIST standard reference database No. 69, 2001.
- Macpherson, G., and Sullivan, P. L. J. C. G.: Dust, impure calcite, and phytoliths: Modeled alternative sources of chemical weathering solutes in shallow groundwater, *Chem Geol*, 527, 118871, 10.1016/j.chemgeo.2018.08.007, 2019.
- Macpherson, G. L.: Hydrogeology of thin limestones: The Konza Prairie Long-Term Ecological Research Site, Northeastern Kansas, *J Hydrol*, 186, 191-228, 10.1016/s0022-1694(96)03029-6, 1996.
- Macpherson, G. L., Roberts, J. A., Blair, J. M., Townsend, M. A., Fowle, D. A., and Beisner, K. R.: Increasing shallow groundwater CO₂ and limestone weathering, Konza Prairie, USA, *Geochimica Et Cosmochimica Acta*, 72, 5581-5599, 10.1016/j.gca.2008.09.004, 2008.
- Nippert, J. B., and Knapp, A. K.: Soil water partitioning contributes to species coexistence in tallgrass prairie, *Oikos*, 116, 1017-1029, 10.1111/j.2007.0030-1299.15630.x, 2007.
- Ransom, M. D., Rice, C. W., Todd, T. C., and Wehmueller, W. A.: Soils and soil biota: *Grassland dynamics: long-term ecological research in tallgrass prairie*. Long-term ecological research network series, Oxford University Press, New York 1998.
- Romero-Mujalli, G., Hartmann, J., Börker, J., Gaillardet, J., and Calmels, D.: Ecosystem controlled soil-rock pCO₂ and carbonate weathering—Constraints by temperature and soil water content, *Chem Geol*, 527, 118634, 10.1016/j.chemgeo.2018.01.030, 2019.
- Tsy-pin, M., and Macpherson, G. L.: The effect of precipitation events on inorganic carbon in soil and shallow groundwater, Konza Prairie LTER Site, NE Kansas, USA, *Applied Geochemistry*, 27, 2356-2369, 10.1016/j.apgeochem.2012.07.008, 2012.
- Veatch, A. M., Dodds, W. K., and Skibbe, A.: Fire and Grazing Influences on Rates of Riparian Woody Plant Expansion along Grassland Streams, *Plos One*, 9, 10.1371/journal.pone.0106922, 2014.
- Vero, S. E., Macpherson, G. L., Sullivan, P. L., Brookfield, A. E., Nippert, J. B., Kirk, M. F., Datta, S., and Kempton, P.: Developing a Conceptual Framework of Landscape and Hydrology on Tallgrass Prairie: A Critical Zone Approach, *Vadose Zone Journal*, 17, 10.2136/vzj2017.03.0069, 2018.
- Wehmueller, W., Ransom, M., and Nettleton, W.: Micromorphology of polygenetic soils in a small watershed, north central Kansas, USA, in: *Developments in Soil Science*, Elsevier, 247-255, 1993.